IEEE Access
Multidisciplinary | Rapid Review | Open Access Journal

Received July 27, 2019, accepted August 25, 2019, date of publication August 29, 2019, date of current version September 13, 2019.

Digital Object Identifier 10.1109/ACCESS.2019.2938255

Selective Sampling and Optimal Filtering for Subpixel-Based Image Down-Sampling

SUNG-HO CHAE, (Student Member, IEEE), SUNG-TAE KIM, JOON-YEON KIM, CHEOL-HWAN YOO, AND SUNG-JEA KO, (Fellow, IEEE)
School of Electrical Engineering, Korea University, Seoul 02841, South Korea

Corresponding author: Sung-Jea Ko (sjko@korea.ac.kr)

This work was supported by the Institute for Information and Communications Technology Promotion (IITP) grant funded by the Korean Government (MSIT) (Intelligent Defense Boundary Surveillance Technology Using Collaborative Reinforced Learning of Embedded Edge Camera and Image Analysis) under Grant 2017-0-00250.

ABSTRACT Subpixel-based image down-sampling has been widely used to improve the apparent resolution of down-sampled images on display. However, previous subpixel rendering methods often introduce distortions, such as aliasing and color-fringing. This study proposes a novel subpixel rendering method that uses selective sampling and optimal filtering. We first generalize the previous frequency domain analysis results indicating the relationships between various down-sampling patterns and the aliasing artifact. Based on this generalized analysis, a subpixel-based down-sampling pattern for each image is selectively determined by utilizing the edge distribution of the image. Moreover, we investigate the origin of the color-fringing artifact in the frequency domain. Optimal spatial filters that can effectively remove distortions caused by the selected down-sampling pattern are designed via frequency domain analyses of aliasing and color-fringing. The experimental results show that the proposed method is not only robust to the aliasing and color-fringing artifacts but also outperforms the existing ones in terms of information preservation.

INDEX TERMS Aliasing, color-fringing, frequency domain analysis, image down-sampling, optimal filtering, selective sampling, subpixel rendering.

I. INTRODUCTION

Most displays, including liquid crystal display (LCD) and organic light-emitting diode (OLED), use red, green, and blue colored components, called subpixels, to represent the color of a pixel. The colors of the three subpixels are recognized as a single color by the human eye because of the blurring effect and spatial integration in the human visual system (HVS) [1]. Therefore, the intensity values of its corresponding subpixels must be appropriately set to display the desired color for a pixel. Subpixel rendering algorithms that control the subpixel values independently have recently been proposed [1]–[15]. Using subpixel rendering, an image with a higher edge sharpness can be achieved by slightly shifting the apparent position of an edge. Also, subpixel-level based approaches have been used to obtain enhanced high-resolution images in some applications, including microscanning [16].

The associate editor coordinating the review of this article and approving it for publication was Madhu S. Nair.

Subpixel rendering techniques have been introduced for image down-sampling required when high-resolution images/videos are displayed on low-resolution displays. While modern cameras offer ultra-high-resolution images of 24.6 MP, and the latest smartphones can take approximately 16 MP images, current displays of digital cameras, smartphones, and monitors have relatively low resolutions (e.g., 2.1 MP on FHD, 3.7 MP on QHD, and 4.3 MP on FHD+ displays). Therefore, image down-sampling is still essential for many devices, and sub-pixel rendering plays an important role. In recent years, subpixel rendering algorithms have been developed to display images without degrading the image quality on displays of various subpixel structures, including the PenTile [17]–[27].

Some high-frequency information that causes the aliasing artifact can be eliminated by filtering the input image before down-sampling [28]. Therefore, previous methods have focused on the filter design for artifact suppression. In [2], the filter coefficients were obtained by solving the optimization problem of which loss function was defined based on the

HVS. Betrisey *et al*. [3] applied the filters in [2] to grayscale font rendering, which is the basis of Microsoft's ClearType. In [4], the subpixel rendering method for the color image was proposed. They utilized filter minimizing chrominance aliasing. Kim and Kim [5] simplified the frequency domain-based optimization problem in [2] by converting to an optimization problem in the spatial domain. However, these methods used the horizontal direct subpixel-based down-sampling (HDSD) and horizontal directional 1D filters; hence, coping with the artifact that occurs in the vertical direction is difficult. In [10], four directional 1D filters, namely horizontal, vertical, diagonal, and anti-diagonal directions, were designed using the optimization-based method. Each filter was applied to the region whose edge direction was perpendicular to the filter. Fang *et al*. [11] introduced the diagonal direct subpixel-based down-sampling (DDSD) that can improve the apparent resolution in both horizontal and vertical directions and 2D filters obtained by extending the 1D optimization problem in [5] to 2D. In [1] and [13], the difference among the direct pixel-based down-sampling (DPD), HDSD, and DDSD were investigated in the frequency domain, and a filter minimizing aliasing was designed via this frequency domain analysis. While the previous methods have concentrated on finding the origin of the aliasing artifact to design an anti-aliasing filter, few analyses of the color-fringing artifact have been performed. Therefore, the filters used in previous methods are limited to cope with the color-fringing artifact.

We propose herein a novel subpixel rendering method that uses selective sampling and optimal filtering. In the proposed method, a subpixel-based down-sampling pattern for each image is selectively determined by utilizing the edge distribution of the image. Optimal spatial filters that can effectively suppress distortions caused by the selected down-sampling pattern are designed via a frequency domain analysis. The remainder of this paper is organized as follows: Section 2 introduces the proposed sampling and filter design methods; Section 3 presents the experimental environment to evaluate the proposed method; and Section 4 provides the concluding remarks.

II. PROPOSED METHOD

We first generalize the previous frequency domain analyses in [1] and [13], which cover the relationships between various down-sampling patterns and the aliasing artifact. We then introduce a selective sampling to determine an appropriate down-sampling pattern for an image based on this generalized analysis. Moreover, we also investigate the origin of the color-fringing artifact in the frequency domain. Finally, using these frequency domain analyses, the design scheme of the optimal spatial filters that can effectively remove both the aliasing and the color-fringing artifacts caused by the selected down-sampling pattern is presented.

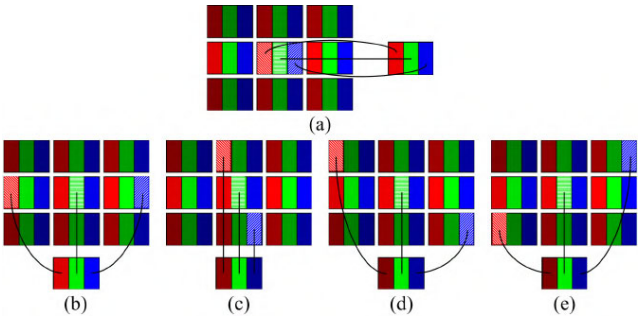

FIGURE 1. Down-sampling patterns: (a) DPD, (b) HDSD, (c) VDSD, (d) DDSD, and (e) ADSD.

A. THE DOWN-SAMPLING METHOD AND THE ALIASING ARTIFACT

Many studies [8], [13], and [29] proved that the aliasing artifact could be reduced by varying the sampling pattern only. For simplicity, we assume that the resolutions of the input and output images are $3M\times3N$ and $M\times N$, respectively, considering that three subpixels correspond to a single pixel. The image down-sampling method can be divided into DPD and direct subpixel based down-sampling (DSD). DSD can provide the resultant image with an improved apparent resolution and a less aliasing artifact [8]. However, DSD suffers from the color distortion phenomenon, called color-fringing artifact. Fig. 1 shows DPD, HDSD, vertical DSD (VDSD), DDSD, and anti-diagonal DSD (ADSD). A suitable down-sampling pattern must be obtained for each image because the tendency of distortions contained in the down-sampled image depends on which down-sampling pattern is used.

As in [13], when the intensity value at the position of (X, Y) in the input image is $C(X, Y)(C \in \{R, G, B\})$, the intensity value at (x, y) in the 3:1 down-sampled image, $C_{\downarrow,3}$ can be represented as follows:

$$\begin{aligned} C_{\downarrow,3}(x,y) = \frac{1}{9} \sum_{X=(3x-2)}^{3x} \sum_{Y=(3y-2)}^{3y} & C(X,Y) \\ & \times (1+2\cos(\frac{2\pi}{3}\cdot X + m_C)) \\ & \times (1+2\cos(\frac{2\pi}{3}\cdot Y + n_C)), \end{aligned} \tag{1}$$

where m_C and n_C are the variables for determining the sampling positions in the horizontal and vertical directions, respectively (e.g., $m_R = n_R = m_G = n_G = m_B = n_B = -4\pi/3$ for DPD, and $m_R = n_R == -2\pi/3, m_G = n_G = -4\pi/3, m_B = n_B = 0$ for DDSD). The discrete-time Fourier transform (DTFT) of (1) is obtained as:

$$\begin{aligned} &\widehat{C}_{\downarrow,3}(u,v) \\ &= \frac{1}{9}\mathbf{1}_3^T \times \begin{bmatrix} \alpha_C^- \cdot \widehat{C}(u^+,v^+) & \beta_C^- \cdot \widehat{C}(u,v^+) & \gamma_C^+ \cdot \widehat{C}(u^-,v^+) \\ \delta_C^- \cdot \widehat{C}(u^+,v) & \widehat{C}(u,v) & \delta_C^+ \cdot \widehat{C}(u^-,v) \\ \gamma_C^- \cdot \widehat{C}(u^+,v^-) & \beta_C^+ \cdot \widehat{C}(u,v^-) & \alpha_C^+ \cdot \widehat{C}(u^-,v^-) \end{bmatrix} \mathbf{1}_3, \end{aligned} \tag{2}$$

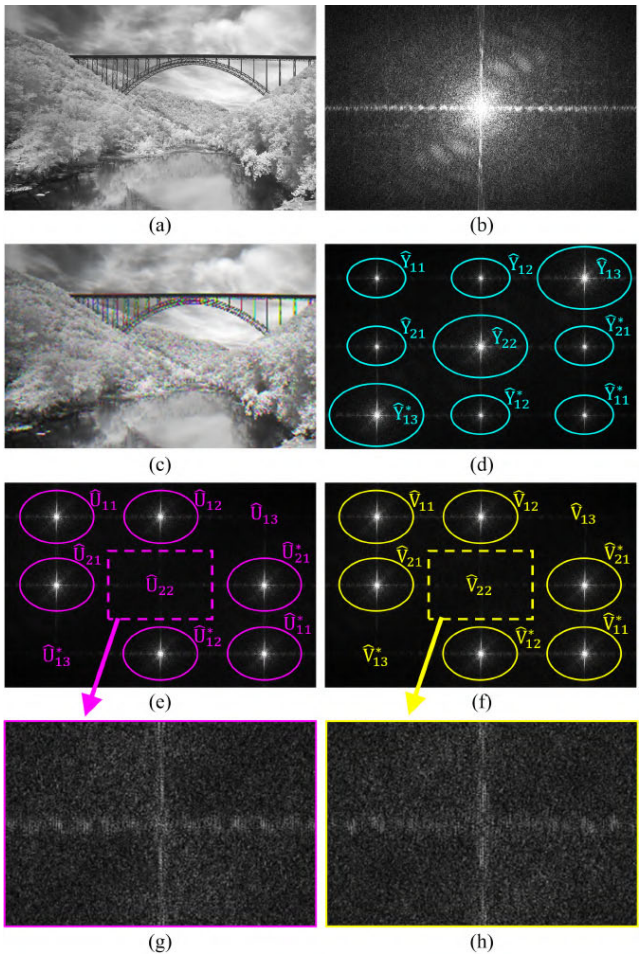

FIGURE 2. Frequency spectra of the input and the result of DDSD. (a) Input image. (b) FS of (a). (c) Result of DDSD. (d) FS of the Y channel of (c). (e) FS of the U channel of (c). (f) FS of the V channel of (c). (g) Magnified FS of $\widehat{\mathrm{U}}_{22}$ in (e). (h) Magnified FS of $\widehat{\mathrm{V}}_{22}$ in (f).

where $\widehat{\mathrm{C}}_{\downarrow,3}$ and $\widehat{\mathrm{C}}$ indicate the frequency spectra (FS) of $\mathrm{C}_{\downarrow,3}$ and C, respectively.

Note that $\mathbf{1}_3 = [1, 1, 1]^T$, $\alpha_{\mathrm{C}}^{\pm} = \exp(\pm j(m_{\mathrm{C}} + n_{\mathrm{C}}))$, $\beta_{\mathrm{C}}^{\pm} = \exp(\pm j \cdot n_{\mathrm{C}})$, $\gamma_{\mathrm{C}}^{\pm} = \exp(\pm j(m_{\mathrm{C}} - n_{\mathrm{C}}))$, $\delta_{\mathrm{C}}^{\pm} = \exp(\pm j \cdot m_{\mathrm{C}})$, $u^{\pm} = u \pm 1/3$, and $v^{\pm} = v \pm 1/3$. For more accurate frequency analysis as described in [13], we convert the RGB color space into the YUV color space as follows:

$$\begin{aligned}\widehat{\mathrm{P}}_{\downarrow,3} &= \sum_{\mathrm{C}\in\{\mathrm{R,G,B}\}} w^{\mathrm{PC}} \cdot \widehat{\mathrm{C}}_{\downarrow,3}, \\ &= \frac{1}{9}\mathbf{1}_3^T \cdot \begin{bmatrix} \widehat{\mathrm{P}}_{11} & \widehat{\mathrm{P}}_{12} & \widehat{\mathrm{P}}_{13} \\ \widehat{\mathrm{P}}_{21} & \widehat{\mathrm{P}}_{22} & \widehat{\mathrm{P}}_{21}^* \\ \widehat{\mathrm{P}}_{13}^* & \widehat{\mathrm{P}}_{12}^* & \widehat{\mathrm{P}}_{11}^* \end{bmatrix} \cdot \mathbf{1}_3, \end{aligned} \tag{3}$$

where w^{PC} is the coefficient for converting from $\mathrm{C} \in \{\mathrm{R, G, B}\}$ to $\mathrm{P} \in \{\mathrm{Y, U, V}\}$ in [30]. Note that $\widehat{\mathrm{P}}_{ij}^*$ is the complex conjugate of $\widehat{\mathrm{P}}_{ij}$. When down-sampling is performed to the input image in the spatial domain, the FS of the down-sampled image is composed of the baseband (BB) and its shifted replicas (SRs) [31]. In (3), $\widehat{\mathrm{P}}_{22}$ is the BB and the remaining components indicate SRs. For DDSD, the FS of the Y, U, and V channels in (3) are illustrated in Figs. 2(d)-(f), respectively. According to the Nyquist-Shannon sampling theorem [32], if the highest frequency contained in the input image is higher than the Nyquist frequency, aliasing occurs because the BB is overlapped with its SRs. When one of the DSDs is used, the phase shift occurs because of $\alpha_{\mathrm{C}}^{\pm}$, $\beta_{\mathrm{C}}^{\pm}$, $\gamma_{\mathrm{C}}^{\pm}$, and $\delta_{\mathrm{C}}^{\pm}$ in (2), and the variance of some SRs in the Y channel decreases. For example, $|\widehat{\mathrm{Y}}_{11}| = |\widehat{\mathrm{Y}}_{12}| = |\widehat{\mathrm{Y}}_{21}| < |\widehat{\mathrm{Y}}_{22}|$ as shown in Fig 2(d). Therefore, more details of the image with DSD can be maintained compared to DPD because the folded region between the BB and some SRs is reduced. Fig. 3 illustrates the down-sampling results of an achromatic image and its corresponding FS of the Y channel in various sampling patterns. While the resultant image of DPD in Fig. 3(b) have some broken edges, the connectivity of the edges can be maintained in the results of some DSDs in Figs. 3(c), 3(e), and 3(f).

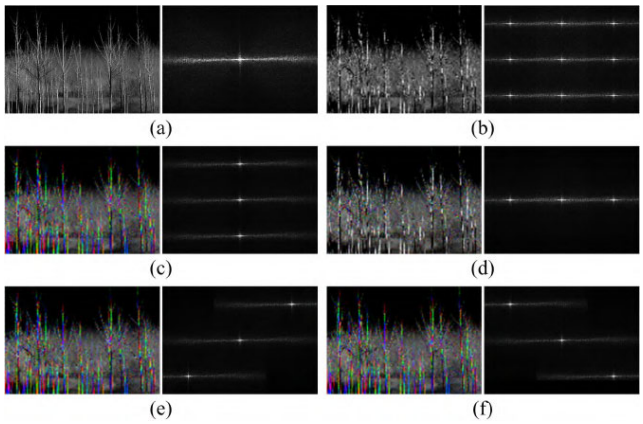

FIGURE 3. Image and the corresponding FS of the Y channel according to each sampling pattern. (a) Input image and its FS. Results of (b) DPD, (c) HDSD, (d) VDSD, (e) DDSD, and (f) ADSD.

B. SELECTIVE SAMPLING

The DSD type determines whether or not the variance of the SR decreases. An appropriate down-sampling pattern for the input image should be chosen to reduce aliasing. For example, if the input image contains many vertical edges, as in Fig. 3(a), the FS is mainly distributed along the horizontal direction. In this case, any DSD, except for VDSD, can reduce the folded region. Similarly, the use of HDSD, DDSD, and ADSD are undesirable for images with horizontal, diagonal, and anti-diagonal edges, respectively.

Selecting either DDSD or ADSD is advantageous in avoiding the inter-signal interference in the frequency domain because, in general, an image mainly consists of vertical or horizontal edges rather than diagonal or anti-diagonal edges. Therefore, we propose herein the selective sampling method to employ either DDSD or ADSD by analyzing the edge distribution of the input image. In the Y channel FS of the input image, when the diagonal variance is greater than the anti-diagonal variance, DDSD is selected. It is because large diagonal variance indicates that the input image contains many anti-diagonal edges. In contrast, if the anti-diagonal

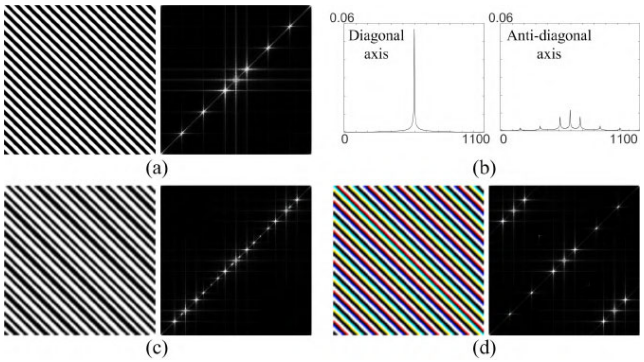

FIGURE 4. Selective sampling. (a) Input image and its FS. (b) Marginal distributions along the diagonal and anti-diagonal axes. (c) Results of DDSD. (e) Results of ADSD.

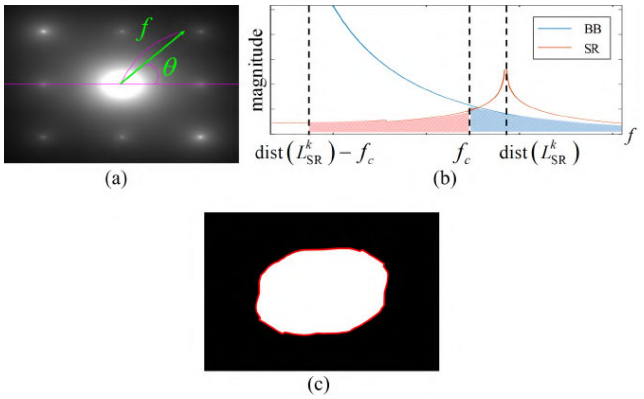

FIGURE 5. Generating an anti-aliasing filter. (a) Fitted 2D Laplace distributions ($\lambda_{BB} = 5$). (b) Cut-off frequency for $\theta = 0$. (c) Proposed anti-aliasing filter.

variance of the FS is greater than the diagonal variance, the proposed selective sampling method adopts ADSD. The entropies of the marginal distributions along the diagonal and anti-diagonal axes are employed to compare the variances. Fig. 4 illustrates an example of selective sampling. The entropy of the marginal distribution along the anti-diagonal axis is larger than that along the diagonal axis in Fig. 4(b); thus, ADSD in Fig. 4(d) is used instead of DDSD in Fig. 4(c).

C. OPTIMAL SPATIAL FILTER DESIGN

The optimal filter consists of an anti-aliasing filter in the Y channel and filters for suppressing the color-fringing artifact in the U and V channels. We first design the anti-aliasing filter via the frequency domain analysis in Section II-A. Then, a method of removing the color-fringing artifact is introduced. Finally, the spatial filters for the R, G, and B channels are generated by color space conversion of the optimal filters in Y, U, and V channels.

In [1], [8], [9], and [13], previous methods designed fixed-shaped, such as circular or rectangular, anti-aliasing filters by considering the trade-off between apparent luminance sharpness and chrominance distortion. However, the fixed-shaped filters can hardly satisfy the optimal cut-off frequency of all directions in the 2D frequency domain. To overcome this problem, we design an arbitrary shaped low-pass filter by considering the bandwidths of the BB and SRs in the Y channel. As described in [1] and [13], the majority of the spectral energy of the natural image is highly concentrated in the lower frequency; therefore, the Laplacian probability density function tends to be a good model for representing the FS. Based on this observation, we apply 2D Laplace distribution fitting to all portions of the Y channel FS for robust analysis. The proposed anti-aliasing filter, $\widehat{f_a}$, minimizes the cost function defined as follows:

$$\arg\min_{\widehat{f_a}} \sum_{k=1}^{8} l_{SR}^{k}(\widehat{f_a}) + \lambda_{BB} \cdot l_{BB}(\widehat{f_a}), \tag{4}$$

where $l_{SR}^{k}(\widehat{f_a})$ and $l_{BB}(\widehat{f_a})$ are the amount of distortion caused by the aliasing artifact from k^{th} SR and the loss of the high-frequency of BB, respectively, and λ_{BB} is the weighting factor that controls the balance between aliasing and blurring. The larger the value of λ_{BB}, the less blurring occurs, but the more influenced it is by the aliasing artifact. The filter in (4) improves the apparent resolution by preserving the high-frequency components of BB and decreases the distortion by minimizing the interference from SRs. Solving (4) is equivalent to finding the cut-off frequency in all 2D directions of the low-pass filter; hence, we consider only the cut-off frequency in the direction θ, f_c, for simplicity, and then (4) can be re-written as follows:

$$\begin{aligned} &\arg\min_{f_c} \sum_{k=1}^{8} l_{SR}^{k,\theta}(f_c) + \lambda_{BB} \cdot l_{BB}^{\theta}(f_c), \\ &l_{SR}^{k,\theta}(f) = \int_{\mathrm{dist}(L_{SR}^{k})-f}^{f} L_{SR}^{k}(r\cdot\cos\theta, r\cdot\sin\theta)dr, \\ &l_{BB}^{\theta}(f) = \int_{f}^{\infty} L_{BB}(r\cdot\cos\theta, r\cdot\sin\theta)dr, \end{aligned} \tag{5}$$

where L_{SR}^{k} and L_{BB} are the fitted 2D Laplace distributions of the k^{th} SR and the BB, respectively. Note that $\mathrm{dist}(L_{SR}^{k})$ indicates the distance between the origin and the center location of the k^{th} SR. Fig. 5 shows the procedure of generating the proposed filter for the image in Fig. 2(a). Fig. 5(a) illustrates the fitted Laplace distributions of the ADSD image, where $\lambda_{BB} = 5$, and Fig. 5(b) shows the process of obtaining f_c. The areas of the red and blue regions in Fig. 5(b) represent $l_{SR}^{k,0}$ and l_{BB}^{0}, respectively. Fig.5(c) presents the proposed anti-aliasing filter.

The previous methods [1], [5], and [8]–[11] employed either only an anti-aliasing filter or a single filter for reducing both the aliasing and color-fringing artifacts instead of using a filter dedicated to removing color-fringing. Therefore, previous filters are limited in terms of coping with the color-fringing artifact. DSD causes an imbalance in the local color, which is commonly called the color-fringing artifact. This artifact is well observed when DSD is applied to the achromatic image. We present herein the origin of the

color-fringing artifact through the frequency domain investigation. If DDSD is applied to an achromatic input image in Fig. 2(a), some SRs, e.g., $\widehat{\mathrm{U}}_{11}$, $\widehat{\mathrm{U}}_{12}$, $\widehat{\mathrm{V}}_{11}$, and $\widehat{\mathrm{V}}_{12}$, etc., contain frequency signals because of the phase shift, and these signals invade the BBs as shown in Figs. 2(g) and 2(h); hence, the color-fringing artifacts appear. In the case of a chromatic image, the BBs in the U and V channels overlap with some SRs of which the distributions are enlarged, yielding color-fringing. To alleviate color-fringing, we directly suppress the frequency components of SRs, which cause the color-fringing artifact, instead of generating any complicated filters. In the U channel, the six SRs among the eight SRs interfere in the BB because of the increased variance. These SRs are classified into two kinds of distributions, namely $\widehat{\mathrm{U}}_1$ and $\widehat{\mathrm{U}}_2$. For the case of DDSD in Fig. 2, $\widehat{\mathrm{U}}_1 = (\widehat{\mathrm{U}}_{11} = \widehat{\mathrm{U}}^*_{21} = \widehat{\mathrm{U}}^*_{12})$ and $\widehat{\mathrm{U}}_2 = (\widehat{\mathrm{U}}_{12} = \widehat{\mathrm{U}}_{21} = \widehat{\mathrm{U}}^*_{11})$ lead to the color-fringing artifact. Similarly, in the V channel, $\widehat{\mathrm{V}}_1$ and $\widehat{\mathrm{V}}_2$ can be designated as the distributions causing color fringing. We apply the ideal low-pass filter, $\widehat{f}_{\mathrm{ideal}}$, to $\widehat{\mathrm{U}}_1$, $\widehat{\mathrm{U}}_2$, $\widehat{\mathrm{V}}_1$, and $\widehat{\mathrm{V}}_2$ as follows to prevent the color-fringing artifact:

$$\begin{aligned}
&\begin{pmatrix}\widehat{\mathrm{U}}'_1\\ \widehat{\mathrm{U}}'_2\\ \widehat{\mathrm{V}}'_1\\ \widehat{\mathrm{V}}'_2\end{pmatrix} = \mathrm{diag}\left(\widehat{f}_{\mathrm{ideal}},\widehat{f}_{\mathrm{ideal}},\widehat{f}_{\mathrm{ideal}},\widehat{f}_{\mathrm{ideal}}\right)\cdot\begin{pmatrix}\widehat{\mathrm{U}}_1\\ \widehat{\mathrm{U}}_2\\ \widehat{\mathrm{V}}_1\\ \widehat{\mathrm{V}}_2\end{pmatrix},\\
&\begin{pmatrix}\widehat{\mathrm{U}}_1\\ \widehat{\mathrm{U}}_2\\ \widehat{\mathrm{V}}_1\\ \widehat{\mathrm{V}}_2\end{pmatrix} = \mathbf{W}_{\mathrm{UV}}\cdot\begin{pmatrix}\widehat{\mathrm{R}}\\ \widehat{\mathrm{G}}\\ \widehat{\mathrm{B}}\end{pmatrix}\\
&\quad = \begin{pmatrix}\eta_{\mathrm{R}}\cdot w_{\mathrm{UR}} & \eta_{\mathrm{G}}\cdot w_{\mathrm{UG}} & \eta_{\mathrm{B}}\cdot w_{\mathrm{UB}}\\ \xi_{\mathrm{R}}\cdot w_{\mathrm{UR}} & \xi_{\mathrm{G}}\cdot w_{\mathrm{UG}} & \xi_{\mathrm{B}}\cdot w_{\mathrm{UB}}\\ \eta_{\mathrm{R}}\cdot w_{\mathrm{VR}} & \eta_{\mathrm{G}}\cdot w_{\mathrm{VG}} & \eta_{\mathrm{B}}\cdot w_{\mathrm{VB}}\\ \xi_{\mathrm{R}}\cdot w_{\mathrm{VR}} & \xi_{\mathrm{G}}\cdot w_{\mathrm{VG}} & \xi_{\mathrm{B}}\cdot w_{\mathrm{VB}}\end{pmatrix}\cdot\begin{pmatrix}\widehat{\mathrm{R}}\\ \widehat{\mathrm{G}}\\ \widehat{\mathrm{B}}\end{pmatrix},\\
&\quad\begin{cases}\eta_{\mathrm{C}} = \exp(j\cdot m_{\mathrm{C}}), \quad \xi_{\mathrm{C}} = \exp(-j\cdot n_{\mathrm{C}}),\\ \qquad\qquad\qquad\qquad\qquad \text{if DDSD},\\ \eta_{\mathrm{C}} = \exp(-j\cdot n_{\mathrm{C}}), \quad \xi_{\mathrm{C}} = \exp(-j\cdot m_{\mathrm{C}}),\\ \qquad\qquad\qquad\qquad\qquad \text{if ADSD},\end{cases}
\end{aligned} \tag{6}$$

where $\widehat{\mathrm{U}}'_1$, $\widehat{\mathrm{U}}'_2$, $\widehat{\mathrm{V}}'_1$, and $\widehat{\mathrm{V}}'_2$ are filtered results of $\widehat{\mathrm{U}}_1$, $\widehat{\mathrm{U}}_2$, $\widehat{\mathrm{V}}_1$, and $\widehat{\mathrm{V}}_2$, respectively, and diag$(\cdot)$ denotes the square matrix with the parameters on the diagonal entries.

The proposed filters are designed in the YUV color space; hence, we need to convert the color space of the proposed filters into an RGB color space. Finally, the filtered image, $\widehat{\mathbf{I}}' = (\widehat{\mathrm{R}}', \widehat{\mathrm{G}}', \widehat{\mathrm{B}}')^T$, obtained by applying the proposed filters to the input image, $\widehat{\mathbf{I}} = (\widehat{\mathrm{R}}, \widehat{\mathrm{G}}, \widehat{\mathrm{B}})^T$, is represented as:

$$\begin{aligned}
\widehat{\mathbf{I}}' &= \mathbf{W}^{-1}\cdot\mathrm{diag}\left(\widehat{f}_{\mathrm{a}},\widehat{f}_{\mathrm{ideal}},\widehat{f}_{\mathrm{ideal}},\widehat{f}_{\mathrm{ideal}},\widehat{f}_{\mathrm{ideal}}\right)\cdot\mathbf{W}\cdot\widehat{\mathbf{I}},\\
\mathbf{W} &= \begin{pmatrix} w_{\mathrm{YR}} & w_{\mathrm{YG}} & w_{\mathrm{YB}}\\ & \mathbf{W}_{\mathrm{UV}} & \end{pmatrix},\\
\mathbf{W}^{-1} &= \mathrm{pinv}(\mathbf{W}),
\end{aligned} \tag{7}$$

where pinv$(\cdot)$ indicates the pseudo-inverse of the matrix. Equation (7) can be summarized as follows:

$$\begin{aligned}
\widehat{\mathbf{I}}' &= \begin{pmatrix}\widehat{f}_{\mathrm{RR}} & \widehat{f}_{\mathrm{RG}} & \widehat{f}_{\mathrm{RB}}\\ \widehat{f}_{\mathrm{GR}} & \widehat{f}_{\mathrm{GG}} & \widehat{f}_{\mathrm{GB}}\\ \widehat{f}_{\mathrm{BR}} & \widehat{f}_{\mathrm{BG}} & \widehat{f}_{\mathrm{BB}}\end{pmatrix}\cdot\widehat{\mathbf{I}},\\
&(\widehat{f}_{\mathrm{RR}}\widehat{f}_{\mathrm{RG}}\widehat{f}_{\mathrm{RB}}\widehat{f}_{\mathrm{GR}}\widehat{f}_{\mathrm{GG}}\widehat{f}_{\mathrm{GB}}\widehat{f}_{\mathrm{BR}}\widehat{f}_{\mathrm{BG}}\widehat{f}_{\mathrm{BB}})^T\\
&\quad = \begin{pmatrix}\mathbf{W}^{\mathrm{a}}_{11}\mathbf{W}^{\mathrm{a}}_{21}\mathbf{W}^{\mathrm{a}}_{31}\mathbf{W}^{\mathrm{a}}_{12}\mathbf{W}^{\mathrm{a}}_{22}\mathbf{W}^{\mathrm{a}}_{32}\mathbf{W}^{\mathrm{a}}_{13}\mathbf{W}^{\mathrm{a}}_{23}\mathbf{W}^{\mathrm{a}}_{33}\\ \mathbf{W}^{\mathrm{i}}_{11}\mathbf{W}^{\mathrm{i}}_{21}\mathbf{W}^{\mathrm{i}}_{31}\mathbf{W}^{\mathrm{i}}_{12}\mathbf{W}^{\mathrm{i}}_{22}\mathbf{W}^{\mathrm{i}}_{32}\mathbf{W}^{\mathrm{i}}_{13}\mathbf{W}^{\mathrm{i}}_{23}\mathbf{W}^{\mathrm{i}}_{33}\end{pmatrix}^T\\
&\qquad\times\begin{pmatrix}\widehat{f}_{\mathrm{a}}\\ \widehat{f}_{\mathrm{ideal}}\end{pmatrix},\\
\mathbf{W}^{\mathrm{a}}_{pq} &= W_{1p}\cdot W^{-1}_{q1},\\
\mathbf{W}^{\mathrm{i}}_{pq} &= W_{2p}\cdot W^{-1}_{q2} + W_{3p}\cdot W^{-1}_{q3} + W_{4p}\cdot W^{-1}_{q4}\\
&\qquad + W_{5p}\cdot W^{-1}_{q5},
\end{aligned} \tag{8}$$

where $\widehat{f}_{\mathrm{C_1C_2}}$ is the filter when the input and output color space are C_2 and C_1, respectively. W_{pq} and W^{-1}_{pq} indicate $(p,q)^{\mathrm{th}}$ elements of $\mathbf{W}$ and $\mathbf{W^{-1}}$ in (7), respectively. As in [3], we ignore the filters, except for $\widehat{f}_{\mathrm{RR}}$, $\widehat{f}_{\mathrm{GG}}$, and $\widehat{f}_{\mathrm{BB}}$, becuase their amplitudes are sufficiently low, and we have:

$$\mathbf{I}' = \mathrm{diag}\,(f_{\mathrm{RR}}*,\quad f_{\mathrm{GG}}*,\quad f_{\mathrm{BB}}*)\cdot\mathbf{I}, \tag{9}$$

where $*$ is the convolution. The spatial filters f_{RR}, f_{GG}, and f_{BB} are the inverse-DFT of $\widehat{f}_{\mathrm{RR}}$, $\widehat{f}_{\mathrm{GG}}$, and $\widehat{f}_{\mathrm{BB}}$, respectively. Frequency filtering process in (7) seems very complicated, but if we get $\widehat{f}_{\mathrm{a}}$ from (4), it is easy to calculate f_{RR}, f_{GG}, and f_{BB} using (8). Therefore, the filtered image $\mathbf{I}'$ is obtained by spatial filtering in (9) without additional transformations in (7).

The proposed method focuses on eliminating the aliasing and color-fringing artifacts; therefore, some down-sampled images may suffer from blurring. To enhance the sharpness of the down-sampled images, we propose additional filters using the un-sharp masking instead of any complicated post-processing. These extra filters are simply obtained by performing convolution between the predefined un-sharp mask and the optimal filters in (9).

III. EXPERIMENTAL RESULTS

A. OBJECTIVE PERFORMANCE MEASURE

The objective performance measure can evaluate the improvement of the apparent luminance resolution and distortion suppression to compare the effectiveness of the proposed method with that of the existing ones. Two measurements in the previous method are adopted: luminance sharpness measure (LSM) [1] and zoomed PSNR (PSNRz) [7]. LSM is the average of the high-frequency energy indicating the improvement of the apparent luminance. PSNRz evaluates the information preservation by measuring the affinity between the down-sampled and original images. These measurements are defined as follows:

$$\mathrm{LSM}(I) = \frac{1}{4}\sum_{k=1}^{4}\|H^k * I\|_1, \tag{10}$$

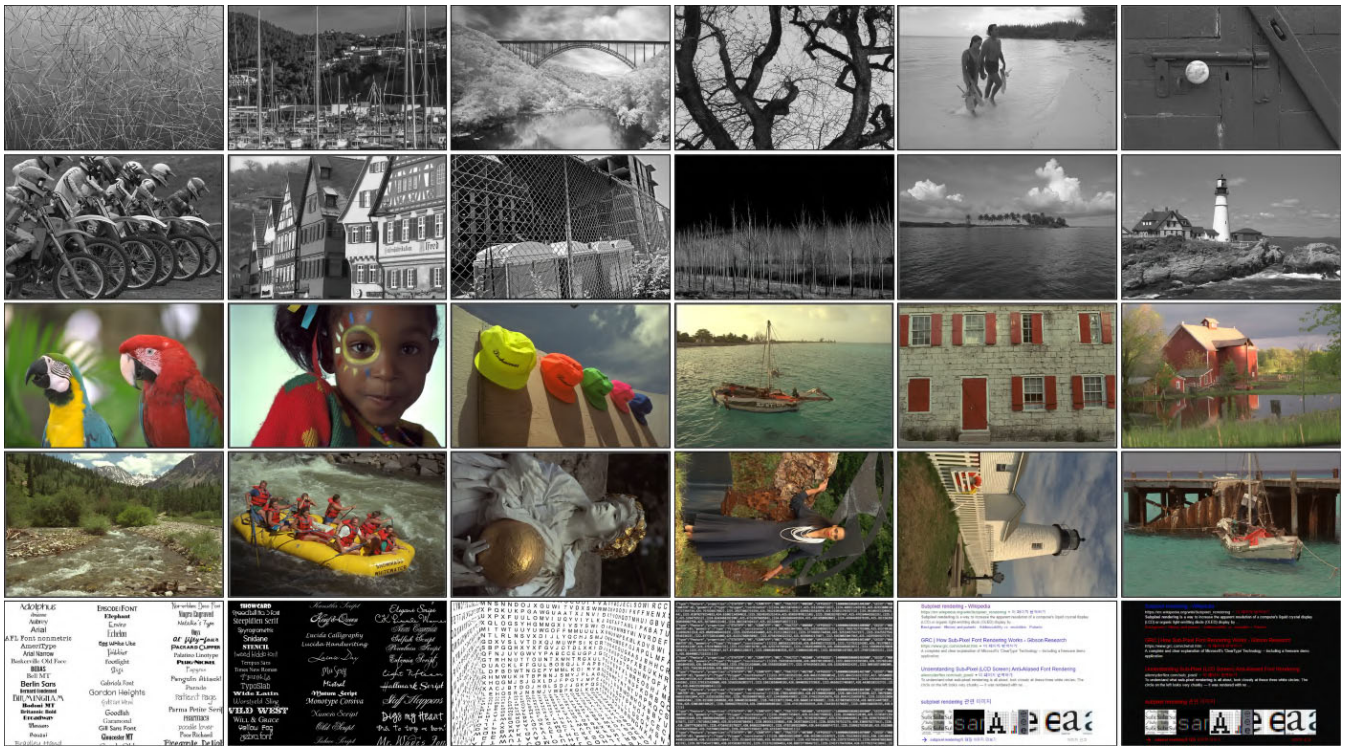

FIGURE 6. Test images used in the experiment, where 1-12 are achromatic images, 13-24 are chromatic images, and 25-30 are text images.

$$\mathrm{PSNRz} = 10\log_{10}\frac{255^2}{\sum_{x,y,c}(I_z(x,y,z) - I_o(x,y,z))^2}, \quad (11)$$

where $H^k = [1, -1]$, $k = \{1, 2, 3, 4\}$ in LSM denotes filters in the horizontal, vertical, diagonal, and anti-diagonal directions. I_z in PSNRz is the zoomed down-sampled image of which the size is equal to that of the original image, I_o. In addition to the previous measures, we propose an aliasing measure (ALM) and a color-fringing measure (CFM) to directly evaluate the suppression of the distortions contained in the down-sampled image. In ALM, we calculate the similarity between the FS of the down-sampled image and that of the original image within the Nyquist frequency as follows:

$$\mathrm{ALM} \triangleq \|\widehat{f}_{\mathrm{ideal}} \cdot (\widehat{Y}_{\downarrow} - \widehat{Y}_o)\|, \quad (12)$$

where $\widehat{Y}_{\downarrow}$ and $\widehat{Y}_o$ represent the Y channel FS of the down-sampled and original images, respectively, and $\|\cdot\|$ is the sum of energy. The smaller ALM indicates less aliasing artifacts. In the CFM, only achromatic images were used to measure the color-fringing more accurately. Since the values of R, G, and B in the achromatic image are the same, the values of R, G, and B in the down-sampled image are also the same if there is no color-fringing artifact. Therefore, CFM is defined as

$$\mathrm{CFM} \triangleq \frac{1}{3}\left(\|I_r - m)\| + \|I_g - m)\| + \|I_b - m)\|\right),$$
$$m(x,y) = (I_r(x,y) + I_g(x,y) + I_b(x,y))/3. \quad (13)$$

The smaller CFM indicates that there are less color-fringing artifacts.

B. EXPERIMENTAL RESULTS

Fig. 6 illustrates the test images used in our experiments. A total of 12 achromatic, 12 chromatic, and six text images were used. λ_{BB} in (4) was set to 5 to acquire the proposed filters. The proposed and proposed with un-sharp masking (proposed-wUM) methods were compared with two direct sampling methods (i.e., DPD and DDSD) and five previous subpixel rendering methods (i.e., Kim and Kim [5], MMDE [10], DDSD-FA [1], MMSE_SD [11], and Kang [14]) to verify effectiveness.

For subjective assessment, Figs. 7–9 depict the cropped results of the achromatic, chromatic, and text images, respectively. The lines in the DPD and AWASR results in Fig. 7 were disconnected because of the aliasing artifact. Many color-fringing artifacts relatively occurred in DDSD, MMDE, and DDSD-FA. While 1D-OSR handled the horizontal artifacts well, it hardly coped with the vertical artifacts. The proposed method managed all artifacts well but resulted in some blurred images. MMSE_SD and the proposed-wUM method had relatively fine results for both artifacts and sharpness. In Fig. 8, the proposed-wUM method had the advantage of preserving the sharpness of the down-sampled image compared with the other methods. Fig. 9 shows that aliasing and color-fringing artifacts affected readability. DPD, 1D-OSR, and AWASR were influenced by aliasing, while DDSD and

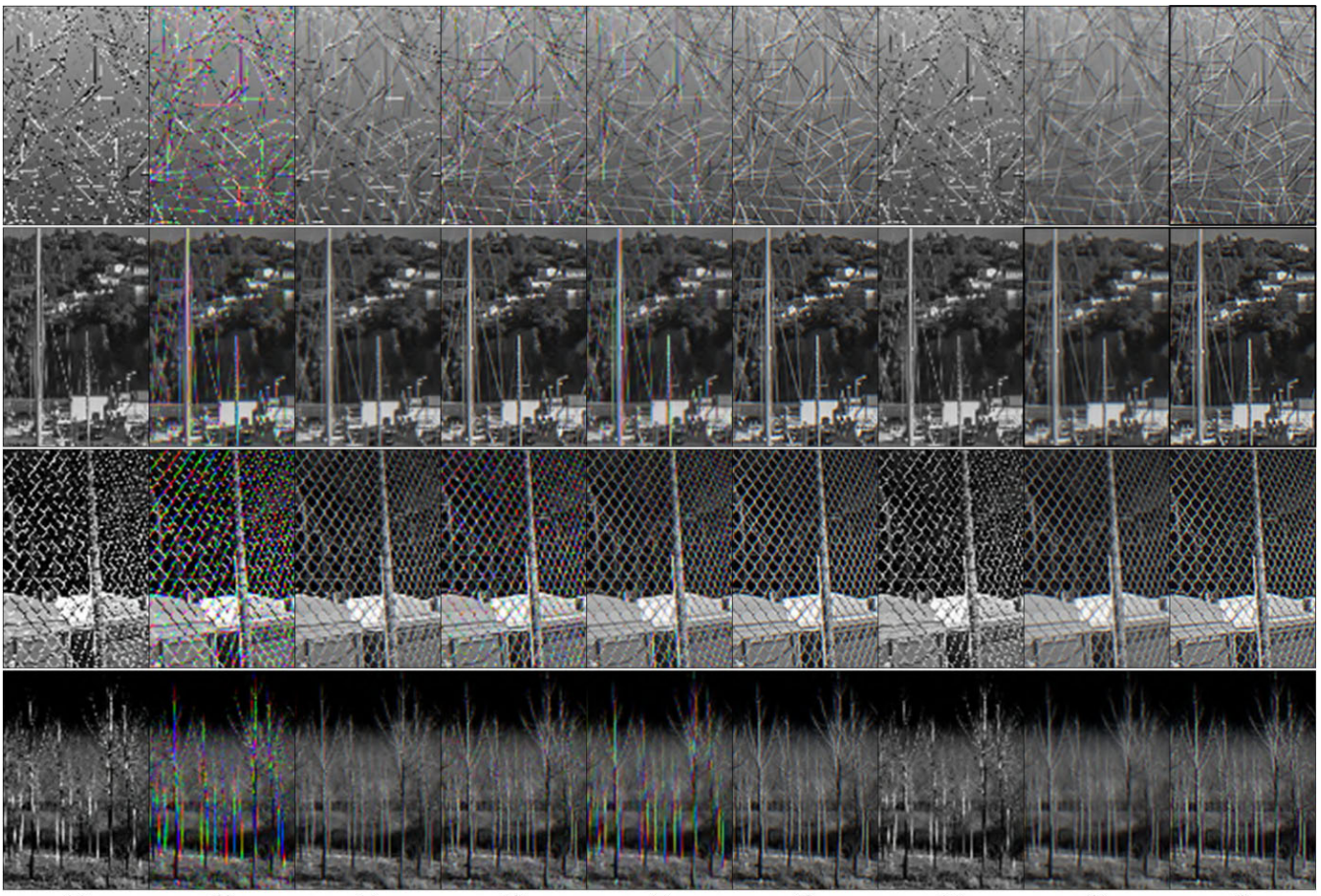

FIGURE 7. Results of the achromatic images: (a) DPD, (b) DDSD, (c) Kim, (d) MMDE, (e) DDSD-FA, (f) MMSE_SD, (g) Kang, (h) proposed, and (i) proposed-wUM.

TABLE 1. LSM.

Image	DPD	DDSD	Kim	MMDE	DDSD-FA	MMSE_SD	Kang	Proposed	Proposed-wUM
Achromatic images	**0.164**	0.145	0.140	0.155	0.136	0.158	0.152	0.123	0.161
Chromatic images	**0.185**	0.160	0.153	0.170	0.150	0.175	0.168	0.133	0.179
Text images	0.177	0.178	0.174	0.191	0.184	0.193	0.177	0.171	**0.199**
Average	0.175	0.158	0.152	0.168	0.151	0.172	0.164	0.137	**0.176**

TABLE 2. PSNRz.

Image	DPD	DDSD	Kim	MMDE	DDSD-FA	MMSE_SD	Kang	Proposed	Proposed-wUM
Achromatic images	19.5	18.8	20.2	20.1	20.3	19.6	20.3	**20.7**	19.7
Chromatic images	23.0	22.3	23.4	23.5	23.7	22.9	23.7	**24.0**	22.9
Text images	14.0	13.3	14.7	14.6	14.6	14.2	14.8	**15.2**	14.4
Average	19.8	19.1	20.4	20.4	20.5	19.8	20.6	**20.9**	19.9

DDSD-FA suffered from the severe color-fringing artifact. MMDE, MMSE_SD, and the proposed-wUM method contained little color-fringing artifacts. The proposed method was the most robust to the artifacts, and the readability of its resultant image was the highest in all the methods.

Tables 1–4 show the objective assessment results. Each table shows LSM, PSNRz, ALM, and CFM in order. The boldface value denotes the highest score in each row, and the underlined value represents the second-highest score. Although the LSM is a good metric for sharpness evaluation, it has a disadvantage of the discontinuity caused by

FIGURE 8. Results of the chromatic images: (a) DPD, (b) DDSD, (c) Kim, (d) MMDE, (e) DDSD-FA, (f) MMSE_SD, (g) Kang, (h) proposed, and (i) proposed-wUM.

TABLE 3. ALM.

Image	DPD	DDSD	Kim	MMDE	DDSD-FA	MMSE_SD	Kang	Proposed	Proposed-wUM
Achromatic images	6.18	3.71	4.23	3.54	**2.21**	2.86	4.69	2.34	3.29
Chromatic images	5.72	3.527	3.65	3.11	2.07	2.75	4.30	**2.05**	2.95
Text images	11.45	7.11	6.05	5.24	4.80	4.26	8.56	**3.87**	4.57
Average	9.76	5.90	5.36	4.74	3.72	4.04	7.17	**3.37**	4.33

TABLE 4. CFM.

Image	DDSD	Kim	MMDE	DDSD-FA	MMSE_SD	Proposed	Proposed-wUM
Achromatic images	646.1	132.0	254.5	229.0	316.3	**124.9**	293.2
Text images	1934.1	**426.9**	688.4	807.0	1084.2	429.1	955.1
Average	968.1	205.8	362.9	373.5	508.3	**200.9**	458.7

aliasing being measured with a high score. Therefore, the best performance in Table 1 seems to be from DPD, but good performances are actually from MMDE, MMSE_SD, and the proposed-wUM method. For PSNRz in Table 2, the proposed method has the best score, which can be interpreted for the same reason that the readability of the proposed results was the highest in Fig. 9. Values of ALM in Table 3 are scaled for convenience of comparison. It is shown that the proposed method is more robust to the aliasing artifact than the other methods. For CFM in Table 4, DPD and AWASR are omitted because the color-fringing artifacts rarely occur in their results. Among the remaining methods, 1D-OSR and the proposed method are significantly less affected by color fringing compared to the other methods. As a result, although

FIGURE 9. Results of the text images: (a) DPD, (b) DDSD, (c) Kim, (d) MMDE, (e) DDSD-FA, (f) MMSE_SD, (g) Kang, (h) proposed, and (i) proposed-wUM.

the sharpness of some down-sampled images of the proposed method is lower than that of the other methods, the proposed method is not only robust to the aliasing and color-fringing artifacts, but also excellent in terms of information preservation. Also, the proposed-wUM can complement the proposed method in situations requiring sharpness.

As for computational complexity, designing the optimal filters and spatial filtering require $O(NlogN)$ and $O(N^2)$ operations, respectively, for the case of N input pixels.

IV. CONCLUSION

This study proposed a novel subpixel rendering method that uses selective sampling and optimal filtering. In the proposed method, a subpixel-based down-sampling pattern for each image was selectively decided by utilizing the edge distribution of the image. An optimal spatial filter based on the selected down-sampling pattern, which can effectively suppress the distortions, was designed via the frequency domain analysis. The experimental results showed that the proposed method is not only robust to the aliasing and color-fringing artifacts, but also outperforms the existing ones in terms of information preservation. Future work will include an extension of the current sampling method. The different sampling method for the different local region is selected by analyzing the contents of the local region in the image, thereby further reduce the local aliasing artifact.

REFERENCES

[1] L. Fang, O. C. Au, K. Tang, and A. K. Katsaggelos, "Antialiasing filter design for subpixel downsampling via frequency-domain analysis," *IEEE Trans. Image Process.*, vol. 21, no. 3, pp. 1391–1405, Mar. 2011.

[2] J. C. Platt, "Optimal filtering for patterned displays," *IEEE Signal Process. Lett.*, vol. 7, no. 7, pp. 179–181, Jul. 2000.

[3] C. Betrisey, J. F. Blinn, B. Dresevic, B. Hill, G. Hitchcock, B. Keely, D. P. Mitchell, J. C. Platt, and T. Whitted, "Displaced filtering for patterned displays," in *SID Symp. Dig. Tech. Papers*, vol. 31, May 2000, pp. 296–299.

[4] D. S. Messing and S. Daly, "Improved display resolution of subsampled colour images using subpixel addressing," in *Proc. Int. Conf. Image Process.*, Rochester, NY, USA, Sep. 2002, pp. 625–628.

[5] J.-S. Kim and C.-S. Kim, "A filter design algorithm for subpixel rendering on matrix displays," in *Proc. 15th Eur. Signal Process. Conf.*, Poznan, Poland, Sep. 2007, pp. 1487–1491.

[6] L. Fang, O. C. Au, X. Wen, Y. Yang, and W. Tang, "An LMMSE-based merging approach for subpixel-based downsampling," in *Proc. 17th Eur. Signal Process. Conf.*, Glasgow, U.K., Aug. 2009, pp. 2254–2257.

[7] K. Tang, O. C. Au, L. Fang, Y. Guo, and J. Pang, "Chroma replacing and adaptive chroma blending for subpixel-based downsampling," in *Proc. IEEE 15th Int. Workshop Multimedia Signal Process. (MMSP)*, Pula, Italy, Sep./Oct. 2013, pp. 212–217.

[8] Y. Ling, O. C. Au, K. Tang, J. Pang, J. Zeng, and L. Fang, "An analytical study of subpixel-based image down-sampling patterns in frequency domain," in *Proc. Vis. Commun. Image Process. (VCIP)*, Kuching, Malaysia, Nov. 2013, pp. 1–6.

[9] J. Zeng, O. C. Au, Y. Guo, J. Pang, K. Tang, and Y. Ling, "Analysis of sampling pattern and Luma-Chroma filter design for subpixel-based image downsampling," in *Proc. IEEE Int. Conf. Acoust., Speech Signal Process. (ICASSP)*, Florence, Italy, May 2014, pp. 5834–5838.

[10] L. Fang and O. C. Au, "Subpixel-based image down-sampling with min-max directional error for stripe display," *IEEE J. Sel. Topics Signal Process.*, vol. 5, no. 2, pp. 240–251, Apr. 2011.

[11] L. Fang, O. C. Au, K. Tang, X. Wen, and H. Wang, "Novel 2-D MMSE subpixel-based image down-sampling," *IEEE Trans. Circuits Syst. Video Technol.*, vol. 22, no. 5, pp. 740–753, May 2012.

[12] L. Fang, O. C. Au, and N.-M. Cheung, "Subpixel rendering: From font rendering to image subsampling," *IEEE Signal Process. Mag.*, vol. 30, no. 3, pp. 177–189, May 2013.

[13] L. Fang, O. C. Au, N.-M. Cheung, A. K. Katsaggelos, H. Li, and F. Zou, "Luma-chroma space filter design for subpixel-based monochrome image downsampling," *IEEE Trans. Image Process.*, vol. 22, no. 10, pp. 3818–3829, Oct. 2013.

[14] S.-J. Kang, "Adaptive weight allocation-based subpixel rendering algorithm," *IEEE Trans. Circuits Syst. Video Technol.*, vol. 24, no. 2, pp. 224–229, Feb. 2013.
[15] S.-J. Kang, "HSI-based color error-aware subpixel rendering technique," *J. Display Technol.*, vol. 10, no. 4, pp. 251–254, 2014.
[16] M.-J. Sun, M. P. Edgar, D. B. Phillips, G. M. Gibson, and M. J. Padgett, "Improving the signal-to-noise ratio of single-pixel imaging using digital microscanning," *Opt. Express*, vol. 24, no. 10, pp. 10476–10485, 2016.
[17] D. S. Messing, L. Kerofsky, and S. Daly, "Subpixel rendering on non-striped colour matrix displays," in *Proc. Int. Conf. Image Process.*, Barcelona, Spain, Sep. 2003, pp. 949–952.
[18] D. S. Messing and L. J. Kerofsky, "Using optimal rendering to visually mask defective Subpixels," *Proc. SPIE*, vol. 6057, pp. 60570O-1–60570O-12, Feb. 2006.
[19] L. Fang, O. C. Au, J. Dai, H. Wang, and N.-M. Cheung, "Analytical study of RGB vertical stripe and RGBX square-shaped subpixel arrangements," in *Proc. 19th IEEE Int. Conf. Image Process.*, Orlando, FL, USA, Sep./Oct. 2012, pp. 333–336.
[20] C. H. B. Elliott, T. L. Credelle, S. Han, M. H. Im, M. F. Higgins, and P. Higgins, "Development of the PenTile Matrix color AMLCD subpixel architecture and rendering algorithms," *J. Soc. Inf. Display*, vol. 11, no. 1, pp. 89–98, Mar. 2003.
[21] M. A. Klompenhouwer and G. D. Haan, "Subpixel image scaling for color-matrix displays," *J. Soc. Inf. Display*, vol. 11, no. 1, pp. 99–108, Mar. 2003.
[22] J. P. Spindler, T. K. Hatwar, M. E. Miller, A. D. Arnold, M. J. Murdoch, P. J. Kane, J. E. Ludwicki, P. J. Alessi, and S. A. Van Slyke, "System considerations for RGBW OLED displays," *J. Soc. Inf. Display*, vol. 14, no. 1, pp. 37–48, Jan. 2006.
[23] J. Pollack, "Displays of a different stripe," *IEEE Spectr.*, vol. 43, no. 8, pp. 40–44, Aug. 2006.
[24] T. Engelhardt, T.-W. Schmidt, J. Kautz, and C. Dachsbacher, "Low-cost subpixel rendering for diverse displays," *Comput. Graph. Forum*, vol. 33, no. 1, pp. 199–209, Feb. 2014.
[25] H.-Y. Yang, J.-S. Lin, and H.-W. Tsao, "The method of 2/3 sampled subpixel rendering for AMOLED display," *J. Display Technol.*, vol. 12, no. 2, pp. 158–164, Feb. 2016.
[26] J. Pang, L. Fang, J. Zeng, Y. Guo, and K. Tang, "Subpixel-based image scaling for grid-like subpixel arrangements: A generalized continuous-domain analysis model," *IEEE Trans. Image Process.*, vol. 25, no. 3, pp. 1017–1032, Mar. 2015.
[27] S.-H. Chae, C.-H. Yoo, J.-Y. Sun, M.-C. Kang, and S.-J. Ko, "Subpixel rendering for the pentile display based on the human visual system," *IEEE Trans. Consum. Electron.*, vol. 63, no. 4, pp. 401–409, Nov. 2017.
[28] E. H. Adelson, C. H. Anderson, J. R. Bergen, P. J. Burt, and J. M. Ogden, "Pyramid methods in image processing," *RCA Eng.*, vol. 29, no. 6, pp. 33–41, 1984.
[29] M.-J. Sun, X.-Y. Zhao, and L.-J. Li, "Imaging using hyperuniform sampling with a single-pixel camera," *Opt. Lett.*, vol. 43, no. 16, pp. 4049–4052, 2018.
[30] *Studio Encoding Parameters of Digital Television for Standard 4:3 and Wide Screen 16:9 Aspect Ratios*, document Rec. ITU-R BT.601-7, 2011.
[31] S. K. Mitra, "Digital processing of continuous-time signals," in *Digital Signal Processing: A Computer-based Approach*, 3rd ed. New York, NY, USA: McGraw-Hill, 2006, ch. 4, pp. 171–231.
[32] R. J. Marks, II, "Generalizations of the sampling theorem," in *Introduction to Shannon Sampling and Interpolation Theory*, 1st ed. New York, NY, USA: Springer-Verlag, 1991, ch. 4, pp. 57–110.

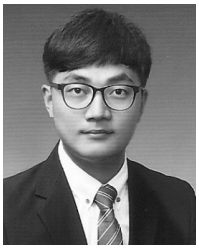

SUNG-HO CHAE received the B.S. degree in electrical engineering from Korea University, Seoul, South Korea, in 2013, where he is currently pursuing the Ph.D. degree in electrical engineering. His research interests include image processing, computer vision, and 3D vision.

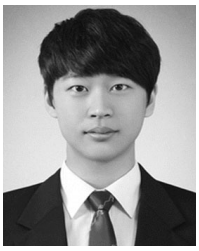

SUNG-TAE KIM received the B.S. degree in electrical engineering from Korea University, in 2013, where he is currently pursuing the Ph.D. degree in electrical engineering. His research interests include human–computer interface, digital signal processing, and computer vision.

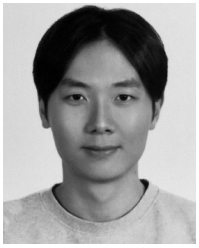

JOON-YEON KIM received the B.S. degree in electrical engineering from Korea University, Seoul, South Korea, in 2014, where he is currently pursuing the Ph.D. degree in electrical engineering. His research interests include computer vision and image processing.

CHEOL-HWAN YOO received the B.S. degree in electrical engineering from Korea University, in 2014, where he is currently pursuing the Ph.D. degree in electrical engineering. His research interests include deep learning, image processing, and computer vision.

SUNG-JEA KO (M'88–SM'97–F'12) received the B.S. degree in electronic engineering from Korea University, in 1980, and the M.S. and Ph.D. degrees in electrical and computer engineering from The State University of New York at Buffalo, in 1986 and 1988, respectively. From 1988 to 1992, he was an Assistant Professor with the Department of Electrical and Computer Engineering, University of Michigan–Dearborn. In 1992, he joined the Department of Electronic Engineering, Korea University, where he is currently a Professor. He has authored over 180 international journal articles. He also holds over 60 registered patents in the fields, such as video signal processing, computer vision, and multimedia communications. He is a Distinguished Lecturer of the IEEE. He was the President of the IEIE, in 2013, and the Vice-President of the IEEE CE Society, from 2013 to 2016. He is a Fellow of the Institution of Engineering and Technology, in 2000. He was a 1999 recipient of the LG Research Award, the Hae-Dong Best Paper Award from the Institute of Electronics and Information Engineers, in 1997, the Best Paper Award from the IEEE Asia–Pacific Conference on Circuits and Systems, in 1996, the Research Excellence Award from Korea University, in 2004, the Technical Achievement Award from the IEEE Consumer Electronics Society, in 2012, the 15-Year Service Award from the TPC of ICCE, in 2014, and the Chester Sall Award from the IEEE CE Society, in 2017. He has served as the General Chairman for ITC-CSCC 2012 and IEICE 2013. He is a member of the Editorial Board of the IEEE TRANSACTIONS ON CONSUMER ELECTRONICS.